

Observation of second-harmonic generation induced by pure spin currents

Lalani K. Werake and Hui Zhao^{*}

Spintronics, where the spin of electrons is used to carry information, is a rapidly growing area of research^{1,2}. There are several techniques for generating pure spin currents^{3–10}; however, there is no method that can directly detect them, largely because they carry no net charge current and no net magnetization. At present, studies of pure spin currents rely on measuring the induced spin accumulation with either optical techniques^{5,11–13} or spin-valve configurations^{14–17}. However, spin accumulation does not directly reflect the spatial distribution or temporal dynamics of the pure spin current, and therefore does not give a real-time or real-space measurement. Here we demonstrate a second-order nonlinear optical effect of the pure spin current that has never been explored before, and show that it can be used for the non-invasive, non-destructive and real-time imaging of pure spin currents. The detection scheme can be applied in a wide range of materials with different electronic band structures because it does not rely on optical resonances. Furthermore, the control of nonlinear optical properties of materials with pure spin currents may have potential applications in photonics integrated with spintronics.

Our experiments are motivated by a recent theoretical prediction of second-order nonlinear optical effects induced by pure spin currents¹⁸. Such an effect originates from a subtle imbalance of the Faraday rotation of electrons with opposite spin orientations. An electron with a certain spin orientation causes Faraday rotation of a linearly polarized light, with an angle determined by the detuning between the frequencies of the light and the interband transition of the electron^{5,11}. In a pure spin current, each electron is accompanied by another electron with an opposite crystal momentum and an opposite spin orientation. The Faraday rotation caused by the two electrons seems to cancel. However, it has been discovered that if the electrons are driven by an optical field, the work done by the intraband acceleration leads to opposite renormalizations to the interband transition frequencies at opposite momenta, because at any particular instant of time, one electron accelerates while the other decelerates¹⁸. Thus, the Faraday rotation caused by the two electrons is not exactly cancelled, leaving a net second-order nonlinear optical susceptibility¹⁸.

We use a quantum interference and control technique¹⁹ to instantaneously inject a pure spin current into a sample with a well-controlled spatial distribution. Specifically, a 400-nm-thick GaAs sample cooled to 10 K is simultaneously illuminated by two laser pulses (see Supplementary Information for details). Electrons can be excited from the valence band to the conduction band by two-photon absorption (red vertical arrows in Fig. 1b) of an \hat{x} -polarized, 75 fs pulse with a central wavelength of 1,500 nm (red waves in Fig. 1) or one-photon absorption (green vertical arrow in Fig. 1b) of a \hat{y} -polarized, 290 fs pulse with a central wavelength of 750 nm (green waves in Fig. 1). Both pulses are incident along the (001) direction of the sample (defined as \hat{z}) and are tightly focused

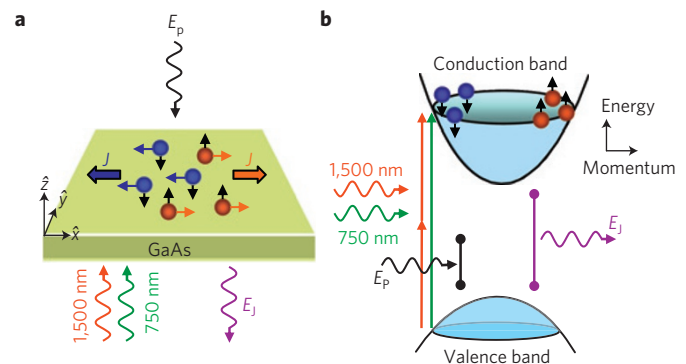


Figure 1 | Schematics of the experimental configuration to observe the second-harmonic generation induced by pure spin currents. a, b, The configuration in real space (a) and energy space (b). The GaAs sample is simultaneously illuminated by two laser pulses (red and green waves). Quantum interference between the transition pathways driven by the two pulses (vertical red and green arrows in b) causes electrons with opposite spin orientations to be excited to energy states with opposite momenta (orange and blue spheres). As the two spin systems move along opposite directions, a pure spin current is formed. The nonlinear optical effect of the injected pure spin current is studied by detecting second-harmonic generation (E_j) from a probe pulse (E_p).

to 2–3 μm (full-width at half-maximum). Owing to the interference of the two transition pathways, electrons with opposite spin orientations along \hat{z} (orange and blue spheres in Fig. 1) are injected with opposite average velocities along \hat{x} . The average velocity, v , and therefore the charge current density of each spin system, J , is proportional to $\cos(\Delta\phi)$, where $\Delta\phi$ is the relative phase between the two transition amplitudes¹⁹. As the charge currents carried by the two spin systems are equal in magnitude but opposite in sign, there is no net charge current along \hat{x} . By analysing the movement of the electrons with a high-resolution pump–probe technique¹³, we roughly estimate that v is of the order of 30 nm ps^{-1} , much higher than a typical drift velocity under an electric field. Hence, even with a moderate carrier density of $1.2 \times 10^{18} \text{ cm}^{-3}$, a very high peak current density of the order of 10^5 A cm^{-2} is achieved.

We demonstrate the second-order nonlinear optical effects of the injected pure spin current by observing a second-harmonic generation process. A 170 fs probe pulse with a central wavelength of 1,760 nm and a pulse energy of 0.1 nJ is incident on the sample along $-\hat{z}$ and is tightly focused to a spot size of 2.1 μm (black waves in Fig. 1). Although the probe pulse propagates along a direction on which the GaAs crystal is centrosymmetric, the inversion symmetry is broken by the pure spin current, allowing second-order optical responses. The second-harmonic pulse induced by the pure spin current has a central wavelength of 880 nm (purple

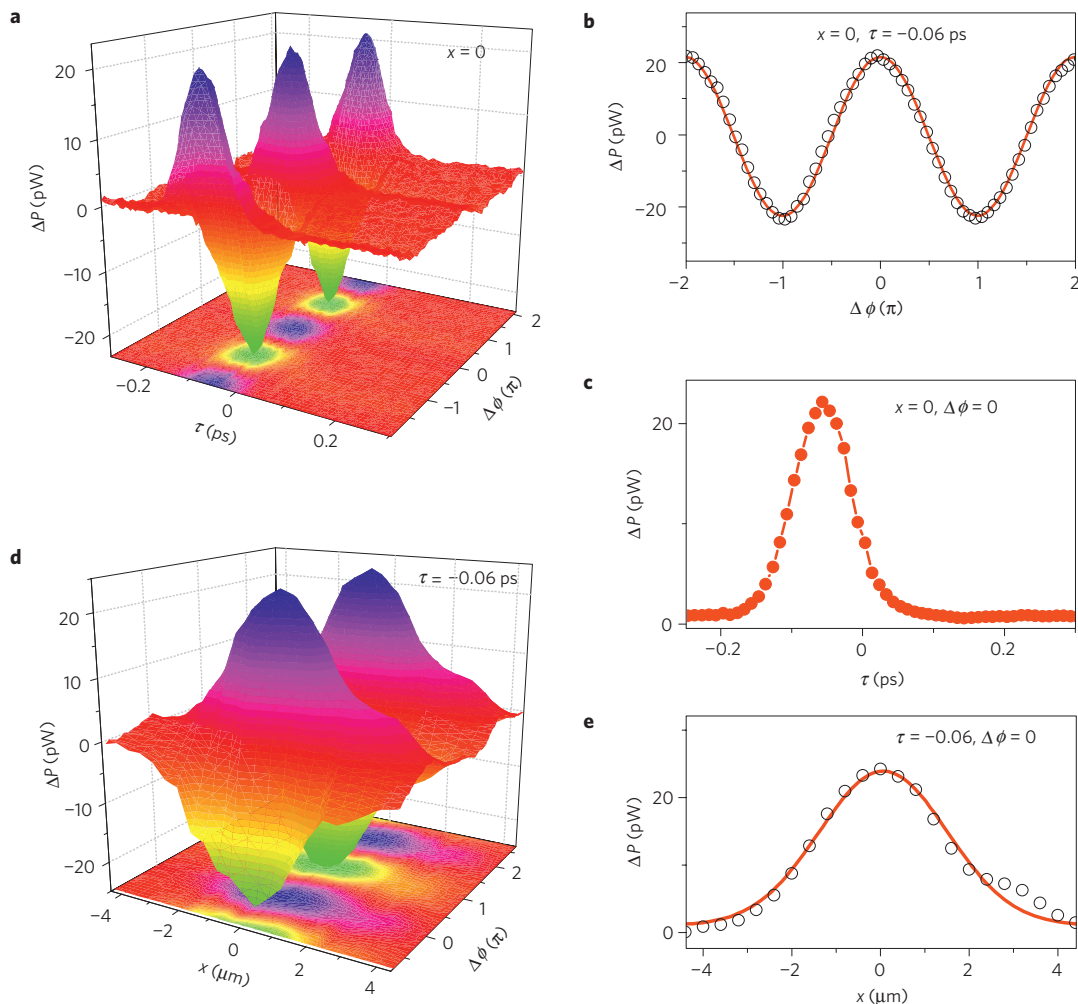


Figure 2 | Second-harmonic generation induced by the pure spin current. **a**, The ΔP measured as functions of the probe delay, τ , and the relative phase, $\Delta\phi$, with the probe and the current-injection spots overlapped ($x = 0$). **b, c**, Cross-sections of **a**, with $\tau = -0.06$ ps (**b**) and $\Delta\phi = 0$ (**c**). **d**, The ΔP measured as functions of x and $\Delta\phi$, with a fixed $\tau = -0.06$ ps. **e**, A cross-section of **d**, with $\Delta\phi = 0$.

waves in Fig. 1), with an amplitude $E_j \propto \chi_j^{(2)} E_p^2$, where E_p is the field amplitude of the probe pulse and $\chi_j^{(2)}$ is the second-order nonlinear susceptibility induced by the spin current. The probe pulse is linearly polarized along \hat{x} , because the most efficient second-harmonic generation occurs when the polarization of the probe light is parallel to the spin current propagation direction¹⁸.

We detect the expected second-harmonic pulse with a coherent detection scheme, where the weak second-harmonic signal is amplified by a vectorial addition with a so-called local oscillator²⁰. The local oscillator has the same frequency and ideally the same phase as the signal, but with a much stronger amplitude E_{LO} . In our experiments, the second-harmonic generated at the sample surface²¹ is used as a natural local oscillator for simplicity. The total second-harmonic intensity is a result of the interference of these two fields: $I = (c\epsilon_0/2)(E_{LO} + E_j)^2$, where c and ϵ_0 are the speed of light and the dielectric constant in a vacuum, respectively. We write this total second-harmonic intensity as $I_{LO} + \Delta I$, where $I_{LO} = (c\epsilon_0/2)E_{LO}^2$ is the intensity of the local oscillator and $\Delta I = (c\epsilon_0/2)(2E_{LO}E_j + E_j^2)$ is the change of the total intensity owing to the pure spin current.

The second-harmonic signal is sent to a silicon photodiode, and the intensity is integrated in both time and space to obtain the average power of the beam. The power corresponding to I_{LO} , P_{LO} , is measured by modulating the intensity of the probe pulse with an optical chopper, with the current-injecting pulses blocked. We

find that $P_{LO} = 4$ nW. The optical power corresponding to ΔI , ΔP , is measured by modulating the average velocity of each spin system, and therefore the current density, with an electro-optic phase modulator²² (see Supplementary Information for details). Under our experimental conditions, the maximum value of ΔP is about 200 times lower than P_{LO} (see Fig. 2), indicating that $E_{LO} \gg E_j$. Therefore, the second term in ΔI is negligible, and $\Delta P \propto \chi_j^{(2)}$.

We measure the ΔP as we systematically vary three controllable parameters in our experiments: the time delay between the peaks of the probe and the current-injecting pulses, τ ; the distance between the centres of the probe and the current-injecting spots, x ; and the relative phase $\Delta\phi$. First, Fig. 2a shows how ΔP varies with τ and $\Delta\phi$, with a fixed $x = 0$. At each τ , $\Delta P \propto \cos(\Delta\phi)$ (Fig. 2b). As $J \propto \cos(\Delta\phi)$, the linear relation between ΔP and J , and therefore between $\chi_j^{(2)}$ and J , is confirmed¹⁸. With a certain $\Delta\phi$, ΔP increases to a peak at about -0.06 ps, and then decays rapidly (Fig. 2c). This temporal behaviour indicates that the relaxation time of the spin current is shorter than the laser pulses at such a high carrier density. Figure 2d shows how ΔP varies with x and $\Delta\phi$, with a fixed $\tau = -0.06$ ps. The same cosine dependence on $\Delta\phi$ is observed at every probe position. At each $\Delta\phi$, ΔP has a Gaussian-like spatial profile (Fig. 2e), consistent with the size and the shape of the laser spots.

The measurements described above are repeated with different carrier densities by adjusting the power of the current-injecting

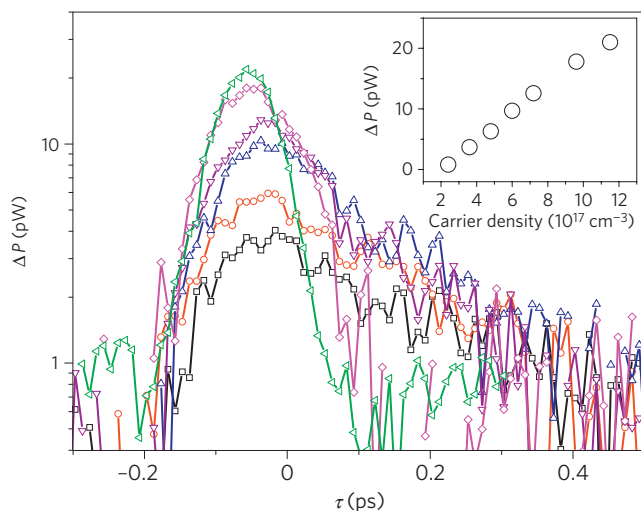


Figure 3 | Time evolutions of ΔP at various carrier densities. The ΔP is measured with $x = 0$ and $\Delta\phi = 0$. The carrier densities are (from bottom (black) to top (green)) 3.6, 4.8, 6.0, 7.2, 9.6 and $12 \times 10^{17} \text{ cm}^{-3}$. The inset shows the height of the peak as a function of carrier density.

pulses. In this way the injected current density is varied by changing the carrier density, while the average velocity is kept unchanged. A few examples are shown in Fig. 3. As we increase the carrier density, the peak shifts to earlier times, and the relaxation after the peak becomes faster. Both features are consistent with a faster relaxation of the spin current owing to an increased carrier scattering rate. Furthermore, as summarized in the inset of Fig. 3, the height of the peak increases with the carrier density. The slight deviation from a linear relation can be attributed to the fact that, although the injected current density is proportional to the carrier density, the current relaxes faster with higher densities, and the height of the peak is determined by both the injection and the relaxation processes.

We have shown in Figs 2 and 3 that the dependencies of the observed second-harmonic signal on the probe delay, the probe position, the average velocity and the carrier density are all consistent with a pure spin current-induced second-harmonic generation process. We have also investigated other possible effects of the current-injecting pulses. First, we can exclude any direct interaction between the laser pulses that does not involve carriers, because the temporal shape of the resulting second harmonic would be independent of the carrier density. This is not what we observed in Fig. 3. The carrier-related effects of the current-injecting pulses include injections of a carrier density, a spin density and a transverse charge current. We have investigated second-harmonic generation owing to each of these on the same sample and under the same conditions, and found that each of them would give a much smaller signal with significantly different temporal behaviours (see Supplementary Information for details).

Accurate determination of the magnitude of this nonlinear effect is difficult because the current density is not precisely known. As a rough estimation, we assume a perfect phase match in the second-harmonic generation, and solve coupled-wave equations²¹. Such a simplification is justified because the sample thickness is smaller than the coherence length. By using the measured P_{LO} and ΔP , we estimate the magnitude of $\chi_1^{(2)}$ to be of the order of 10^{-13} – $10^{-14} \text{ m V}^{-1}$ with $J = 10^5 \text{ A cm}^{-2}$. The direction of the pure spin current can be determined by measuring the dependence of the second-harmonic signal on the polarization of the probe pulse, because the maximum second-harmonic signal is expected when the probe pulse is polarized along the direction of the current¹⁸. The sign of the pure spin current is related to the sign of $\chi_1^{(2)}$,

which can be determined in a coherent detection scheme with a phase-controlled local oscillator.

The demonstrated second-order nonlinear optical effect is large enough to detect low-density spin currents. We choose the probe photon energy to be less than half of the energy bandgap of the sample, so that neither the two-photon absorption of the probe pulse nor the one-photon absorption of the second-harmonic pulse is allowed. Therefore, the probe pulse will not disturb the spin current by injecting extra carriers. However, one could tune the probe photon energy towards the interband transition frequency of the electrons to increase $\chi_1^{(2)}$ (ref. 18). In our experiments, a high-repetition-rate (82 MHz) laser system is used. With high-density spin currents of the order of 10^5 A cm^{-2} , the probe beam with an average power of 10 mW generates second-harmonic signals of the order of 10 pW. Owing to the quadratic dependence of the second-harmonic field amplitude on the probe field amplitude, the second-harmonic generation process can be significantly enhanced with amplified laser systems with lower repetition rates. For example, a 1-kHz laser system with the same average power (commercially available) will increase the second-harmonic power by about five orders of magnitude. Therefore, a typical pure spin current of 1 A cm^{-2} generated by, for example, the spin Hall effect⁵, will induce the same 10-pW second-harmonic signal. The detection can also be significantly improved by replacing the silicon photodiode with a photodetector with femtowatt detectability, which are widely available. Furthermore, the coherent nature of the second-harmonic pulse allows amplification of the signal by using a strong local oscillator in the coherent detection. In our experiments, the second harmonic generated at the sample surface is used as the local oscillator for simplicity. When necessary, the signal can be further amplified by using an externally generated strong second-harmonic pulse.

We have demonstrated second-harmonic generation induced by pure spin currents, and used it for the fast, non-invasive and non-destructive imaging of pure spin currents. Although optical interband absorptions are used to generate the pure spin currents for our demonstration experiment, the detection scheme does not rely on optical resonances. Therefore, it can be generally applied to a wide range of materials with indirect bandgaps or with bandgaps that are too small or too large for absorption-based optical detection techniques. Finally, as a pure spin current is composed of two spin-polarized charge currents with opposite spin polarizations and opposite propagation directions, each component contributes to half of the nonlinear susceptibility¹⁸. Therefore, although we detected pure spin currents in our experiments, this technique can also be used to study spin-polarized charge currents.

Received 21 January 2010; accepted 30 June 2010;
published online 8 August 2010

References

- Wolf, S. A. *et al.* Spintronics: A spin-based electronics vision for the future. *Science* **294**, 1488–1495 (2001).
- Žutić, I., Fabian, J. & Das Sarma, S. Spintronics: Fundamentals and applications. *Rev. Mod. Phys.* **76**, 323–410 (2004).
- Jedema, F. J., Filip, A. T. & van Wees, B. J. Electrical spin injection and accumulation at room temperature in an all-metal mesoscopic spin valve. *Nature* **410**, 345–348 (2001).
- Watson, S. K., Potok, R. M., Marcus, C. M. & Umansky, V. Experimental realization of a quantum spin pump. *Phys. Rev. Lett.* **91**, 258301 (2003).
- Kato, Y. K., Myers, R. C., Gossard, A. C. & Awschalom, D. D. Observation of the spin Hall effect in semiconductors. *Science* **306**, 1910–1913 (2004).
- Ganichev, S. D. *et al.* Zero-bias spin separation. *Nature Phys.* **2**, 609–613 (2006).
- Seki, T. *et al.* Giant spin Hall effect in perpendicularly spin-polarized FePt/Au devices. *Nature Mater.* **7**, 125–129 (2008).
- Uchida, K. *et al.* Observation of the spin Seebeck effect. *Nature* **455**, 778–781 (2008).
- Yang, T., Kimura, T. & Otani, Y. Giant spin-accumulation signal and pure spin-current-induced reversible magnetization switching. *Nature Phys.* **4**, 851–854 (2008).

10. Frolov, S. M., Venkatesan, A., Yu, W., Folk, J. A. & Wegscheider, W. Electrical generation of pure spin currents in a two-dimensional electron gas. *Phys. Rev. Lett.* **102**, 116802 (2009).
11. Kikkawa, J. M. & Awschalom, D. D. Lateral drag of spin coherence in gallium arsenide. *Nature* **397**, 139–141 (1999).
12. Stotz, J. A. H., Hey, R., Santos, P. V. & Ploog, K. H. Coherent spin transport through dynamic quantum dots. *Nature Mater.* **4**, 585–588 (2005).
13. Zhao, H., Smirl, A. L. & van Driel, H. M. Temporally and spatially resolved ballistic pure spin transport. *Phys. Rev. B* **75**, 075305 (2007).
14. Johnson, M. & Silsbee, R. H. Interfacial charge–spin coupling: Injection and detection of spin magnetization in metals. *Phys. Rev. Lett.* **55**, 1790–1793 (1985).
15. Lou, X. H. *et al.* Electrical detection of spin transport in lateral ferromagnet-semiconductor devices. *Nature Phys.* **3**, 197–202 (2007).
16. Tombros, N., Jozsa, C., Popinciuc, M., Jonkman, H. T. & van Wees, B. J. Electronic spin transport and spin precession in single graphene layers at room temperature. *Nature* **448**, 571–574 (2007).
17. van't Erve, O. M. J. *et al.* Electrical injection and detection of spin-polarized carriers in silicon in a lateral transport geometry. *Appl. Phys. Lett.* **91**, 212109 (2007).
18. Wang, J., Zhu, B. F. & Liu, R. B. Second-order nonlinear optical effects of spin currents. *Phys. Rev. Lett.* **104**, 256601 (2010).
19. Bhat, R. D. R. & Sipe, J. E. Optically injected spin currents in semiconductors. *Phys. Rev. Lett.* **85**, 5432–5435 (2000).
20. Hobbs, P. C. D. *Building Electro-Optical Systems* (John Wiley, 2009).
21. Boyd, R. W. *Nonlinear Optics* 3rd edn (Academic, 2008).
22. Ruzicka, B. A. & Zhao, H. Power dependence of pure spin current injection by quantum interference. *Phys. Rev. B* **79**, 155204 (2009).

Acknowledgements

We thank J. Wang, B-F. Zhu and R-B. Liu for sharing their results before publication and acknowledge R-B. Liu for discussions on the experimental approaches and explaining to us the physics mechanisms of the effect. We thank J. Prineas for providing us with high-quality GaAs samples. This material is based on work supported by the National Science Foundation of USA under grant no. DMR-0954486.

Author contributions

L.K.W. constructed the experimental apparatus and carried out the measurements; H.Z. proposed the topic, provided guidance on the experiments and prepared the manuscript. Both authors contributed to data analysis and interpretations.

Additional information

The authors declare no competing financial interests. Supplementary information accompanies this paper on www.nature.com/naturephysics. Reprints and permissions information is available online at <http://npg.nature.com/reprintsandpermissions>. Correspondence and requests for materials should be addressed to H.Z.